JOURNAL OF CATALYSIS 126, 126–146 (1990)

One- and Two-Component Diffusion in Zeolite ZSM-5

I. Theoretical

WAQAR R. QURESHI[1] AND JAMES WEI

Department of Chemical Engineering, Massachusetts Institute of Technology, Cambridge, Massachusetts 02139

Received October 4, 1989; revised March 26, 1990

The properties of a multicomponent diffusion matrix, derived from a model for single-file diffusion, are discussed. This matrix has several pleasing characteristics, many of which can be discussed in terms of its eigenfunctions. The model has been applied to the steady-state Wicke–Kallenbach and to the transient uptake experiments. For the transient uptake, both constant pressure and variable pressure boundary conditions have been considered. Finally, the case of a first-order reversible reaction is addressed. © 1990 Academic Press, Inc.

INTRODUCTION

Several previous workers have developed models for the diffusion of molecules in zeolites. Barrer and Jost (*1*) used an approach based on the concepts of irreversible thermodynamics. Habgood (*2*) extended this concept to two-component systems. Riekert (*3*) and Palekar and Rajadhyakhsha (*4–6*) have used lattice models for some special cases of one- and two-component diffusion. Theodorou and Wei (*7*) modeled the diffusive process as a random walk on a square two-dimensional grid. Tsikoyiannis (*8*) and Tsikoyiannis and Wei (*9*) further developed this model and calculated the diffusional fluxes on the basis of first-order correlation functions. These predicted fluxes are, as expected, identical to the fluxes calculated by Sundaresan and Hall (*10*) from their lattice gas model for the case of negligible interactions between molecules.

The lattice models are based on the idea that molecules are localized within the zeolite lattice and hop from one localized center to the next. This concept is in agreement with recent NMR and powder diffraction experiments on the motion of aromatic molecules in ZSM-5 (*11–15*).

Derouane (*16*) has proposed a model based on the surface curvature of the zeolite, and suggested that molecular shape-selective effects are not necessarily restricted to the intracrystalline volume of zeolites. Derouane *et al.* (*17*) used this model to calculate the physisorption energy for a molecule on a curved surface, and extended the argument by saying that diffusion is controlled by a surface sorption barrier. The model predicts that diffusion rates increase as molecule and pore sizes match each other more intimately. This model may apply in some cases but it does contradict, for example, data collected by several previous workers and correlated by Moore and Katzer (*18*).

In this paper we analyze the properties of the diffusion matrix (Eq. (6)) of Tsikoyiannis (*8*) and Sundaresan and Hall (*10*) for multicomponent systems.

The model of Tsikoyiannis (*8*) assumes that molecules hop in a random fashion on a two-dimensional lattice with the following rules:

1. Molecules hop from intersection to intersection on the grid; the probability that

[1] Present address: Chevron Research and Technology Company, Richmond, CA 94802.

0021-9517/90 $3.00

they will be found in between intersections is negligible.

2. Each hopping event is an independent Poisson process.

3. No more than one particle can occupy a site at a given time.

4. If a molecule is activated, and is destined to hop onto a site that is already occupied by another molecule, then both molecules remain where they are.

The diffusion equation predicted by this model for a one-component system at the level of first-order correlation functions is simply Fick's second law of diffusion,

$$\frac{\partial \theta}{\partial t} = D\,\nabla^2\theta, \tag{1}$$

where the diffusion coefficient for a one-component system is given by

$$D = \alpha^2 q. \tag{2}$$

Here, θ is the occupancy of the component (number of molecules per intersection), α is the distance between intersections, and q is the hopping rate of a molecule (in an otherwise empty lattice) to a specific adjacent site. The corresponding equilibrium equation is given by the Langmuir Isotherm for one-component systems:

$$\theta = \frac{p/q}{1 + p/q + p/q}. \tag{3}$$

Here, p can be interpreted as the bombardment rate of the species onto the grid boundary.

As an example, consider the case of diffusion purely along the x axis in a slab. Then Eq. (1) becomes the familiar expression

$$\frac{\partial\,\theta}{\partial t} = \alpha^2 q \left[\frac{\partial^2\theta}{\partial\,x^2}\right]. \tag{4}$$

We present the above equations for completeness and clarity. In this work we are interested in multicomponent systems and we largely restrict our discussion to such systems.

Figure 1 shows an example of two-component diffusion on the model grid. In this illustration, the component 1 molecules were initially in the grid. The component 2 molecules were then introduced into the gas phase around the grid (ZSM-5 crystals). As equilibrium is approached, the component 2 molecules diffuse into the grid as the component 1 molecules diffuse out. Clearly, there will be some mutual hinderance between the component 1 and 2 molecules as they diffuse in different directions in the grid. It is this kind of problem that we address in this study.

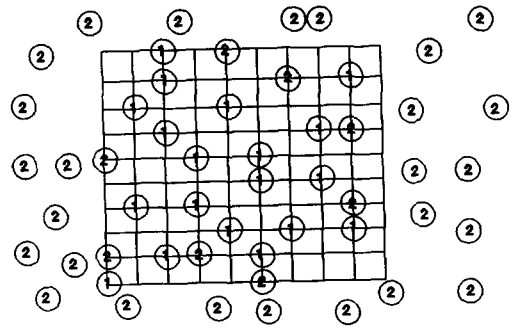

FIG. 1. An example of counter-diffusion on the two-dimensional grid.

The result for the simultaneous diffusion of two components at the level of first-order correlation functions is

$$\frac{\partial\,\underline{\theta}}{\partial t} = \nabla[\mathbf{D}\,\nabla\underline{\theta}], \tag{5}$$

where the constitutive matrix for two-component diffusion, $\mathbf{D}$, is given by

$$\mathbf{D} = \alpha^2 \begin{bmatrix} q_1 & 0 \\ 0 & q_2 \end{bmatrix} \begin{bmatrix} (1-\theta_2) & \theta_1 \\ \theta_2 & (1-\theta_1) \end{bmatrix} \tag{6}$$

and $\underline{\theta}$ is the occupancy vector

$$\underline{\theta} = \begin{bmatrix} \theta_1 \\ \theta_2 \end{bmatrix}. \tag{7}$$

In these equations, q_i can be interpreted as the hopping rate of a molecule of component i (in an otherwise empty lattice) to a specific adjacent site.

The partitioning implied by this model is given by

$$\theta_i = \frac{p_i/q_i}{1 + p_1/q_i + p_2/q_2} \quad i = 1, 2, \quad (8)$$

where p_i can be interpreted as the bombardment rate of the ith component onto the grid boundary. Equation (8) is simply a Langmuir Isotherm for a two-component system.

For the majority of this paper we use vector notation as it allows results to be presented in a concise manner. However, note that Eq. (5) could be expressed without using vector notation as the simultaneous equations

$$\partial\theta_1/\partial t = \alpha^2 q_1[(1 - \theta_2)\,\nabla^2\theta_1 + \theta_1\,\nabla^2\theta_2] \quad (9)$$

$$\partial\theta_2/\partial t = \alpha^2 q_2[\theta_2\,\nabla^2\theta_1 + (1 - \theta_1)\,\nabla^2\theta_2]. \quad (10)$$

The appropriate expression for $\nabla^2\theta_i$ is given by the particular problem being considered. For example, for diffusion in a slab purely along the x axis,

$$\nabla^2\theta_i = \left[\frac{\partial^2\,\theta_i}{\partial x^2}\right]. \quad (11)$$

The detailed description of the derivation of Eqs. (1) and (5) and considerable discussion of the model are given in both Tsikoyiannis and Wei (*9*) and Tsikoyiannis (*8*).

It is important to note that the above model has been developed at the microscale level with certain basic assumptions of the diffusion mechanism. It can now be used to make predictions of the macroscopic and observable behavior of two-component diffusion.

Qureshi and Wei (*19*) compare predictions given by the equations developed above with results from experiments on the counterdiffusion and codiffusion of benzene and toluene in zeolite ZSM-5. To get a good comparison with experimental data, it was necessary to accurately model the constant volume, variable pressure boundary conditions that existed in the experimental setup. However, before analyzing this transient uptake, variable pressure case, we consider two simpler cases to illustrate the properties of the diffusion matrix. These are steady-state diffusion in a Wicke–Kallenbach cell and transient uptake with constant pressure boundary conditions. The Wicke–Kallenbach cell, in particular, demonstrates several very appealing properties, and we have included an initial section, Illustrative Examples, to briefly demonstrate some of these features. Finally, we consider the case of a first-order, reversible reaction to evaluate the implications of this model on the most important industrial usage of ZSM-5, as a catalyst.

PROPERTIES OF THE D MATRIX

Illustrative Examples

The **D** matrix given in Eq. (6) for two components has some remarkable properties, which can be explored by considering, as shown in Fig. 2, a Wicke–Kallenbach experiment of steady-state diffusion through a porous membrane. The matrix has two eigenvalues, and we designate λ_f and λ_s as the fast and slow eigenvalues, respectively. Let $\nabla\theta_1$ and $\nabla\theta_2$ be the concentration gradients of components 1 and 2 in the crystal. Then, if the concentration gra-

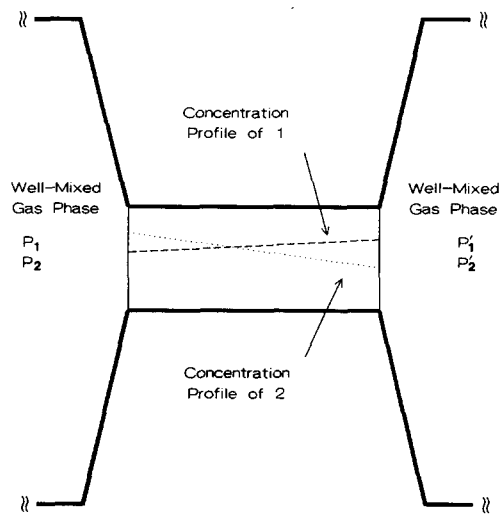

FIG. 2. The Wicke–Kallenbach diffusion cell.

dient ratio, that is, $\nabla\theta_1/\nabla\theta_2$ is equal to the slope of an eigenvector, the flux is in the opposite direction to that eigenvector on the θ_1, θ_2 plane. The eigenvectors $\underline{X}_f$ and $\underline{X}_s$ are designated as the fast and slow modes of diffusion, respectively.

In all of the following analyses, for the purpose of clarity, we put $\alpha = 1$ unless otherwise explicitly stated.

Take as an example $q_1 = q_2 = 1$. In this case, the two eigenvalues and the associated eigenvectors become simply

The fast mode: $\lambda_f = 1$, $\underline{X}_f = (\theta_1, \theta_2)$

The slow mode: $\lambda_s = 1 - \theta_1 - \theta_2$, $\underline{X}_s = (1, -1)$.

The fast mode is simply codiffusion where the gradients are proportional to the occupancies, or concentrations; the slow mode is counterdiffusion where the gradients are equal and opposite. Since these are pure modes, we label these states of "pure codiffusion" and "pure counterdiffusion," respectively. The very agreeable interpretation, as demonstrated in Fig. 3, is that the more rapid diffusivity of pure codiffusion is independent of occupancy. The slower diffusivity of pure counterdiffusion declines with occupancy according to $(1 - \theta)$; it corresponds to self-diffusion, and is a case of equimolar counterdiffusion as discussed by Riekert (*3*).

For a numerical example, take $\underline{\theta} = (\theta_1, \theta_2) = (0.3, 0.2)$; the diffusion matrix becomes

$$\mathbf{D} = \begin{bmatrix} 0.8 & 0.3 \\ 0.2 & 0.7 \end{bmatrix}$$

which has eigenfunctions $\lambda_f = 1$, $\lambda_s = 0.5$, $\underline{X}_f = (0.3, 0.2)$, and $\underline{X}_s = (1, -1)$. In the codiffusion case, the gradients are $\nabla\underline{\theta} = (0.3, 0.2)$, resulting in a flux of $\underline{J} = (-0.3, -0.2)$, which is large and has the opposite vector direction as the occupancy or gradient. In a counterdiffusion case where the gradient is $\nabla\underline{\theta} = (0.2, -0.2)$, the resulting flux is $\underline{J} = (-0.1, 0.1)$, which is small and

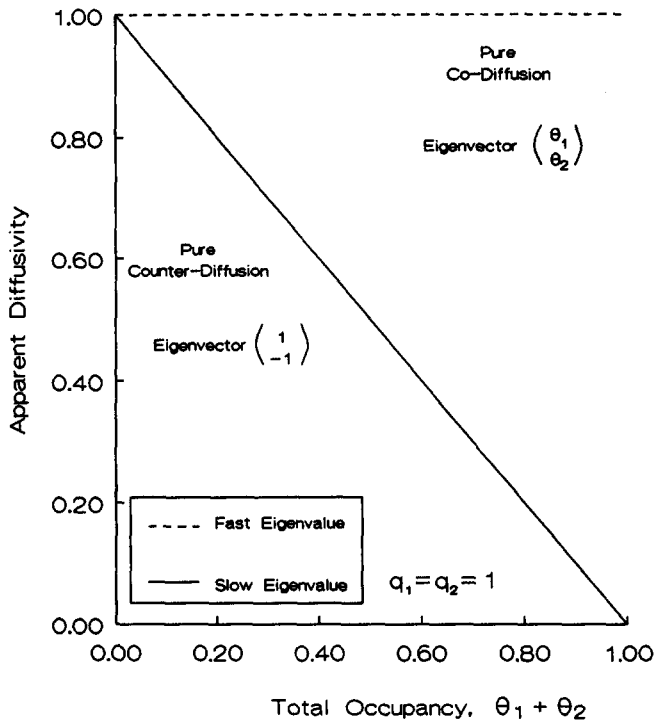

FIG. 3. Fast and slow eigenvalues for both hopping rates equal to 1.

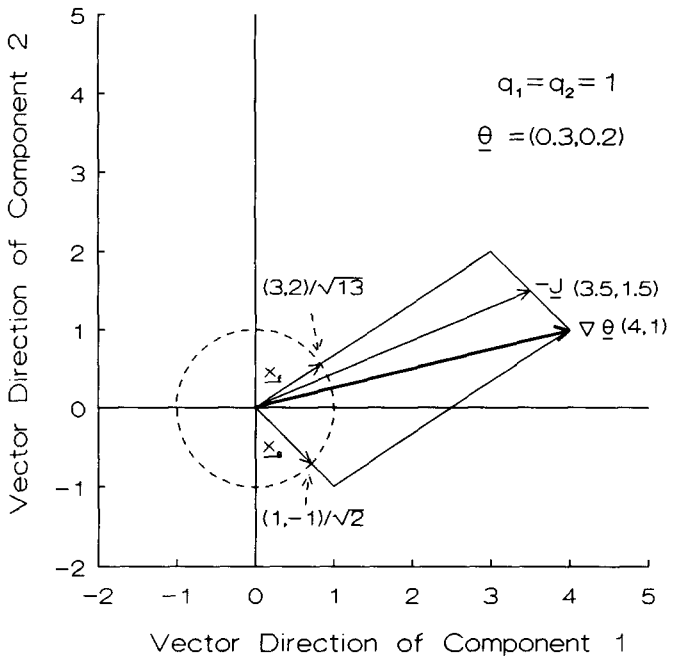

FIG. 4. A numerical example of the eigenvector representation of the flux and occupancy gradient vectors on the occupancy plane.

has the opposite vector direction as the gradient. Any arbitrary gradient is a linear combination of the eigenvectors, as is the flux. We can normalize the eigenvectors to get an idea of whether an arbitrary gradient is closer to co- or counterdiffusion. In general we have

$$\nabla\underline{\theta} = C_f\underline{x}_f + C_s\underline{x}_s \tag{12}$$

$$-\underline{J} = \mathbf{D}\,\nabla\underline{\theta} = C_f\lambda_f\underline{x}_f + C_2\lambda_s\underline{x}_s. \tag{13}$$

So, for the case given above, we have $\underline{x}_f = (3, 2)/\sqrt{13}$, and $\underline{x}_s = (1, -1)/\sqrt{2}$, and if for example $\nabla\underline{\theta} = (4, 1) = \sqrt{13}\underline{x}_f + \sqrt{2}\underline{x}s$, we can say that the gradient is closer to being codiffusion than counterdiffusion. The associated flux is $\underline{J} = (-3.5, -1.5)$ or $-\underline{J} = (3.5, 1.5)$ as illustrated in Fig. 4.

Precisely the same consideration applies to three- or multicomponent systems. For a three-component system we have

$$\mathbf{D} = \begin{bmatrix} q_1 & 0 & 0 \\ 0 & q_2 & 0 \\ 0 & 0 & q_3 \end{bmatrix} \begin{bmatrix} 1-\theta_2-\theta_3 & \theta_1 & \theta_1 \\ \theta_2 & 1-\theta_3-\theta_1 & \theta_2 \\ \theta_3 & \theta_3 & 1-\theta_1-\theta_2 \end{bmatrix}. \tag{14}$$

In the simple case of equal jumping rates $q_1 = q_2 = q_3 = 1$, the fast eigenvalue is $\lambda_f = 1$, which is independent of occupancy, and the associated eigenvector is $(\theta_1, \theta_2, \theta_3)$, which represents codiffusion where all the gradients are proportional to the occupancy. There is a double eigenvalue of $\lambda_{s1} = \lambda_{s2} = 1 - \theta_1 - \theta_2 - \theta_3$, which declines linearly with total occupancy, and has the associated eigenvectors $\underline{X}_{s1} = (1, -1, 0)$ and $\underline{X}_{s2} = (0, 1, -1)$ which span all the counterdiffusion gradients by linear combinations.

In the case of unequal jumping rates there is a rotation of the eigenvectors. The

interpretations of codiffusion and counterdiffusion remain unchanged, although now, the slow mode is not equimolar counterdiffusion. For example, let $q_1 = 1$ and $q_2 = 1.5$, and again take $\underline{\theta} = (0.3, 0.2)$; then the diffusion matrix and the associated eigenfunctions are

$$\mathbf{D} = \begin{bmatrix} 0.8 & 0.3 \\ 0.3 & 1.05 \end{bmatrix}$$

$$\lambda_f = 1.25 \quad \underline{x}_f = (2, \quad 3)/\sqrt{13}$$

$$\lambda_s = 0.6 \quad \underline{x}_s = (3, -2)/\sqrt{13}.$$

The fast mode is still codiffusion, but weighted in favor of the faster component 2; and the slow mode is still counterdiffusion, but weighted in favor of the slower component 1. See Fig. 5.

Apparent Diffusion Coefficient

The **D** matrix predicts that the flux of a component is a function of the concentrations and concentration gradients of both components. So in general

$$J_i = f_i(\nabla\theta_1, \nabla\theta_2, \theta_1, \theta_2), \quad i = 1, 2 \quad (15)$$

For example, for the Wicke–Kallenbach cell,

$$\underline{J} = -\mathbf{D}\,\nabla\underline{\theta}. \quad (16)$$

However, the measurement that is usually made experimentally is of an apparent diffusion coefficient, which, for the case of a Wicke–Kallenbach cell, is defined by

$$D_i^{\dagger} = -J_i/\nabla\theta_i, \quad i = 1, 2 \quad (17)$$

For the transient uptake case, we define the apparent diffusion coefficients by first obtaining the "approach to equilibrium versus time curves" from the model. Next, we fit to those curves the curves generated by the usual Fickean diffusion equations, with the only fitted parameters being the apparent diffusivities.

So, in detail, we first define the approach to equilibrium versus time curves as

$$\chi_i(t) = (\bar{\theta}_i(t) - \bar{\theta}_{i0})/(\bar{\theta}_{i\infty} - \bar{\theta}_{i0}), \quad (18)$$

where $\bar{\theta}_i(t)$ is the volumetric average occupancy, defined by

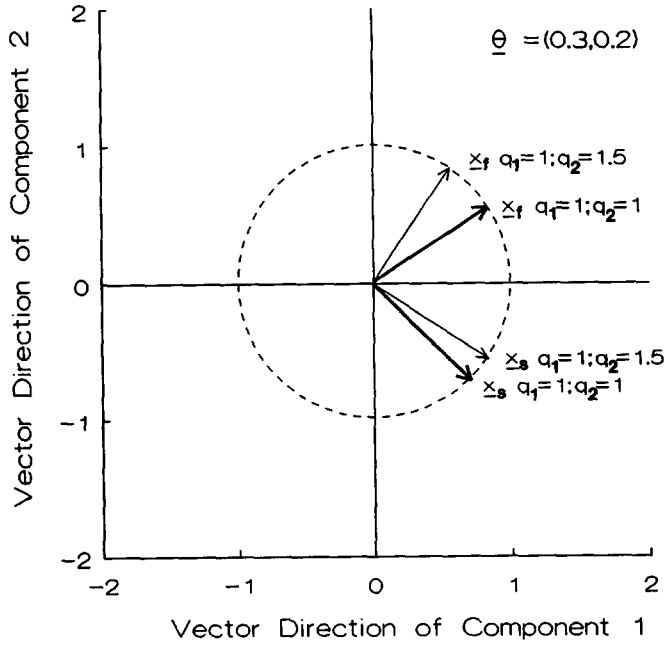

FIG. 5. The rotation of eigenvectors on the occupancy plane caused by changing the hopping rates.

$$\bar{\theta}_i(t) = \frac{\int \theta_i(t)\, dV}{V}. \tag{19}$$

The $\chi_i(t)$ are obtained from the model's diffusion equation

$$\frac{\partial \underline{\theta}}{\partial t} = \nabla(\mathbf{D} \nabla \underline{\theta}) \tag{20}$$

together with the initial conditions

$$\underline{\theta}_i = \underline{\theta}_{i0}, \quad t = 0, i = 1, 2, \tag{21}$$

and in the constant pressure case we have fixed boundary conditions

$$\underline{\theta}_i = \underline{\theta}_{ib}, \quad r = R, i = 1, 2. \tag{22}$$

Or in the case of the constant volume, variable pressure situation the boundary conditions are given by

$$\theta_i = \frac{K_i P_i}{1 + K_1 P_1 + K_2 P_2}, \quad r = R, i = 1, 2 \tag{23}$$

$$\frac{V_g}{R_g T} \frac{\partial P_i}{\partial t} = -m\rho \frac{\partial \bar{\theta}_i}{\partial t}, \quad i = 1, 2, \tag{24}$$

where m is the grams of crystals, ρ is the moles of intersections per gram of crystals, V_g is the gas phase volume, R_g is the gas law constant, and T is the temperature.

Now, to the generated $\chi_i(t)$ we fit the corresponding curves generated by the usual Fickean diffusion equation

$$\frac{\partial \underline{\theta}}{\partial t} = \nabla(\mathbf{D}^\dagger \nabla \underline{\theta}), \tag{25}$$

where

$$\mathbf{D}^\dagger = \begin{bmatrix} D_1^\dagger & 0 \\ 0 & D_2^\dagger \end{bmatrix}. \tag{26}$$

The initial and boundary conditions are once again given by Eqs. (21) and (22) for the constant pressure case, and Eqs. (21), (23), and (24) for the variable pressure case.

The only parameters allowed to vary in this fitting are $D_1^\dagger$ and $D_2^\dagger$, the two apparent diffusion coefficients. The fitting is usually performed over the range 10 to 90% approach to equilibrium.

We use this concept of an apparent diffusivity as it is an advantageous method to enable understanding of many of the theoretical predictions, as well as a practical way of comparing experimental and theoretical results. Thus, $D_i^\dagger$ depends on the concentrations and concentration gradients of both components, and gives us a means of interpreting experimental results in terms of those variables.

Wicke–Kallenbach

We now consider the Wicke–Kallenbach type diffusion cell of Fig. 2 in more detail. The catalyst crystal in the cell provides the only pathway for mass transfer between two well-mixed gas phases. Each gas phase contains fixed concentrations of the two components being studied. The system is at steady state, so there is a constant flux of each component through the crystal. The concentration gradients are assumed to be very small and hence linear.

Apparent diffusion coefficients, $D_i^\dagger$, can be calculated for each of the two diffusing components

$$D_i^\dagger = \frac{-J_i}{d\theta_i/dx} = q_i \alpha^2 \left[(1 - \theta_j) + \theta_i \left[\frac{(d\theta_j/dx)}{(d\theta_i/dx)}\right]\right], \quad i, j = 1, 2, i \neq j. \tag{27}$$

Figure 6 shows $D_1^\dagger$ as a function of the ratio of the gradient of component 2, $d\theta_2/dx$, to the gradient of component 1, $d\theta_1/dx$, for different values of their occupancies, θ_1 and θ_2. The figure assumes $\alpha = 1$ and $q_1 = 1$. Two series of lines are shown. The first has $\theta_1 = 0.1$ and $\theta_2 = 0.1$, 0.45, and 0.8. This series shows the effect of varying the occupancy of component 2. The second series has $\theta_2 = 0.1$, and $\theta_1 = 0.1$, 0.45, and 0.8, and shows the effect of varying component 1. The line $\theta_1 = \theta_2 = 0.1$ is common to both series. The figure illustrates that changing θ_2 varies the intercept, and changing θ_1 varies the slope of each line, as each line has a slope of θ_1 and an intercept of $1 -$

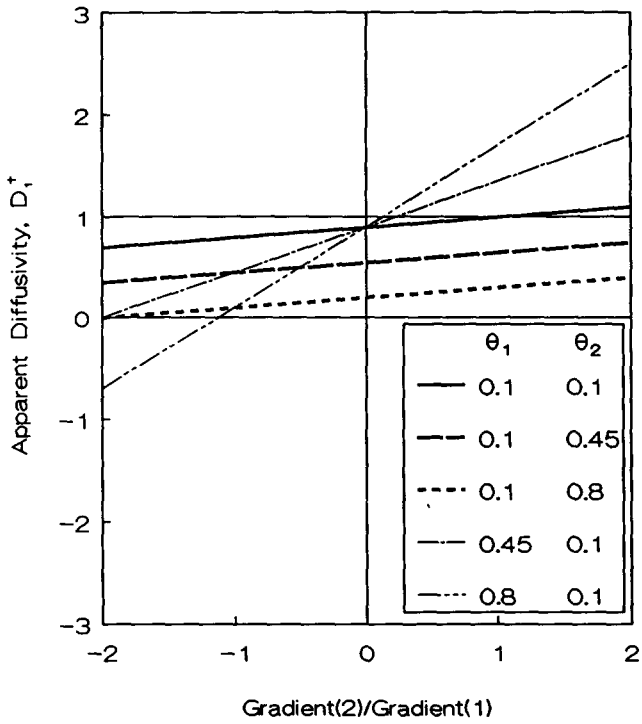

FIG. 6. Apparent diffusivity of component 1 in the Wicke–Kallenbach cell: $D_1^\dagger = (1 - \theta_2) + \theta_1[(d\theta_2/dx)/(d\theta_1/dx)]$.

θ_2. This means that as the occupancy of component 1 is increased the gradient ratio has a greater affect on $D_1^\dagger$, and $D_1^\dagger$ decreases with increasing θ_2. An important point to note is that the flux of component 1 can actually go up against its own concentration gradient, resulting in a negative apparent diffusivity. This occurs when the gradient of component 2 is much larger and in the opposite direction to the gradient of component 1. Finally, note that $D_1^\dagger$ is not a function of q_2, although, of course, it is a function of q_1.

Eigenfunction Representation

The underlying structure of the diffusion matrix is such that if the concentration gradients across the Wicke–Kallenbach cell are set up in the same ratio as the slope of one of the eigenvectors, then the apparent diffusivities of both components will be equal to the eigenvalue corresponding to that eigenvector.

Figure 7 shows both $D_1^\dagger$ and $D_2^\dagger$ as functions of the ratio of $d\theta_2/dx$ to $d\theta_1/dx$ for $\theta_1 = \theta_2 = 0.1$, and for hopping rates of 1. This is one form of graphical depiction of the **D** matrix. The points of intersection between the curves for $D_1^\dagger$ and $D_2^\dagger$ are of importance. It is at these two points that the apparent diffusivities are equal to the eigenvalues of the diffusion matrix, and the concentration gradient ratio is equal to the slope of the eigenvectors.

In the general case, the diffusion matrix from the stochastic model has eigenvalues:

$$\lambda = \{q_1(1 - \theta_2) + q_2(1 - \theta_1) \pm [q_1^2(1 - \theta_2)^2 + q_2^2(1 - \theta_1)^2 + 2q_1q_2(\theta_1\theta_2 + \theta_1 + \theta_2 - 1)]^{1/2}\}/2 \quad (28)$$

with corresponding eigenvectors

$$\underline{X} = \begin{bmatrix} u \\ v \end{bmatrix},$$

where

$$v = -\frac{(q_1(1 - \theta_2) - \lambda)u}{q_1\theta_1}. \qquad (29)$$

The larger eigenvalue is designated the fast eigenvalue and the smaller eigenvalue is called the slow eigenvalue.

The fast eigenvalue has the property of being the maximum attained by the minimum of the functions $D_1^\dagger$ and $D_2^\dagger$. Similarly the slow eigenvalue is the minimum value attained by the maximum of the functions $D_1^\dagger$ and $D_2^\dagger$. A consequence of these relationships is that for any particular gradient ratio at most only one component can have an apparent diffusivity exceeding the fast eigenvalue; further, it is only when the gradient ratio is equal to the fast eigenvector that both apparent diffusivities are equal to the fast eigenvalue. Analogous reasoning can be made for the slow eigenvalue. That is, at most only one component can attain an apparent diffusivity lower than the slow eigenvalue, and both components can attain the slow eigenvalue only when the gradient ratio is equal to the slow eigenvector slope.

Several important results can be derived from manipulating Eqs. (27)–(29). First, it can be shown that the diffusion matrix is positive semidefinite; that is, both the slow and fast eigenvalues are always greater than or equal to 0. Second, the fast eigenvalue always corresponds to a case of codiffusion; that is, both fluxes are in the same direction and the corresponding eigenvector, $\underline{X}_f$, has a positive slope. Similarly, the slow eigenvalue corresponds to a case of counterdiffusion; that is, the fluxes are in opposite directions and the corresponding eigenvector, $\underline{X}_s$, has a negative

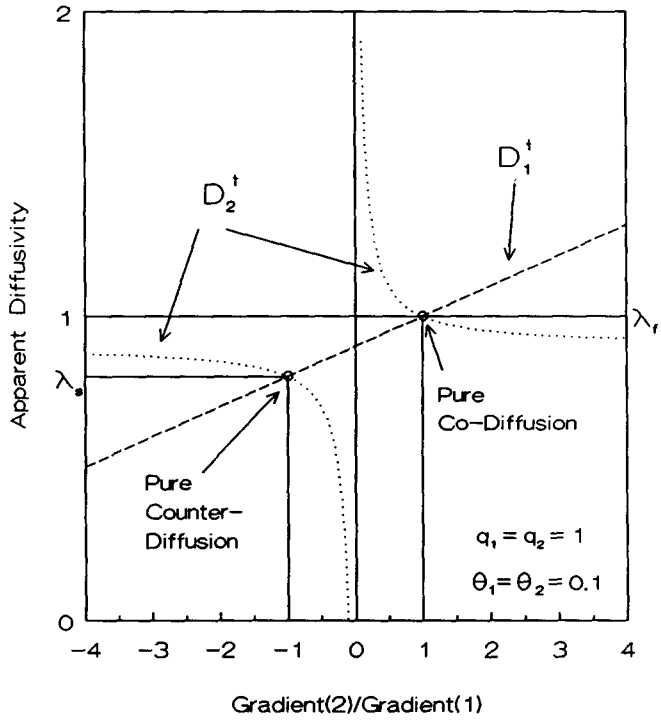

FIG. 7. Apparent diffusivities of components 1 and 2 in the Wicke–Kallenbach cell: $D_1^\dagger = 0.9 + 0.1[(d\theta_2/dx)/(d\theta_1/dx)]$; $D_2^\dagger = 0.9 + 0.1[(d\theta_1/dx)/(d\theta_2/dx)]$.

slope. Finally, for any situation where the concentration gradients are in opposite directions, the apparent diffusivities of both components are less than their respective hopping rates.

Figure 7 is specific for particular hopping rates and occupancies. It would be useful to be able to generalize this depiction. One way to do this is to consider the intersection points, that is, the eigenvectors and eigenvalues as being representative of the figure. Then we can use Figs. 8 and 9 to determine the fast and slow eigenvalues as functions of the hopping rate of component 2, and Figs. 10 and 11 to obtain the corresponding eigenvectors. Thus, Figs. 8 and 9 give the ordinates for the points of intersection, and Figs. 10 and 11 give the abscissas.

For example, consider the case $\theta_1 = \theta_2 = 0.1$, $q_1 = 1$, and $q_2 = 10$. Then, from Figs. 8–11, $\lambda_f = 9.0$, $\lambda_s = 0.89$, and the slopes of $\underline{X}_f$ and $\underline{X}_s$ are 81 and -0.12, respectively. This immediately shows that the fast mode, or pure codiffusion state, is achieved when the gradient of component 2 is 81 times greater than the gradient of component 1. In this state the faster component 2 entrains component 1, and the resulting apparent diffusivity of both components is 9.0. In the slow mode, or pure counterdiffusion state, the gradient of component 2 is 0.12 times the gradient of component 1, and in the opposite direction. In this case, component 1 is slowing down component 2 and the apparent diffusivity of both components is 0.89. The behavior of this system at all gradient ratios can be seen in Fig. 12, which is analogous to Fig. 7 except the hopping rate of component 2 is now 10.

Figures 8–11 each showed the same two series of lines that were shown in Fig. 3. That is, the first series is $\theta_1 = 0.1$ and $\theta_2 = 0.1$, 0.45, and 0.8, and the second is $\theta_2 = 0.1$ and $\theta_1 = 0.1$, 0.45, and 0.8. It can be observed from these figures that both the fast and slow eigenvalues (that is, the pure

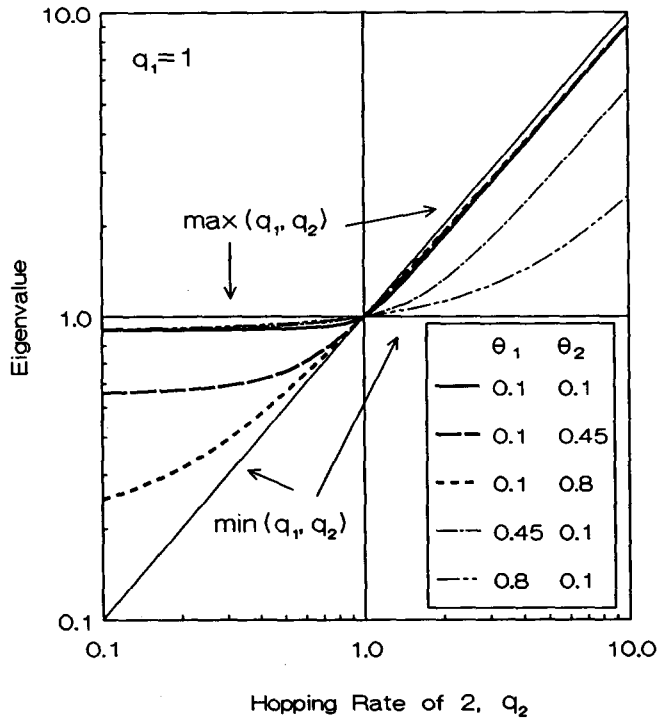

FIG. 8. The fast eigenvalue. Note that $\min(q_1, q_2) \leq \lambda_f \leq \max(q_1, q_2)$.

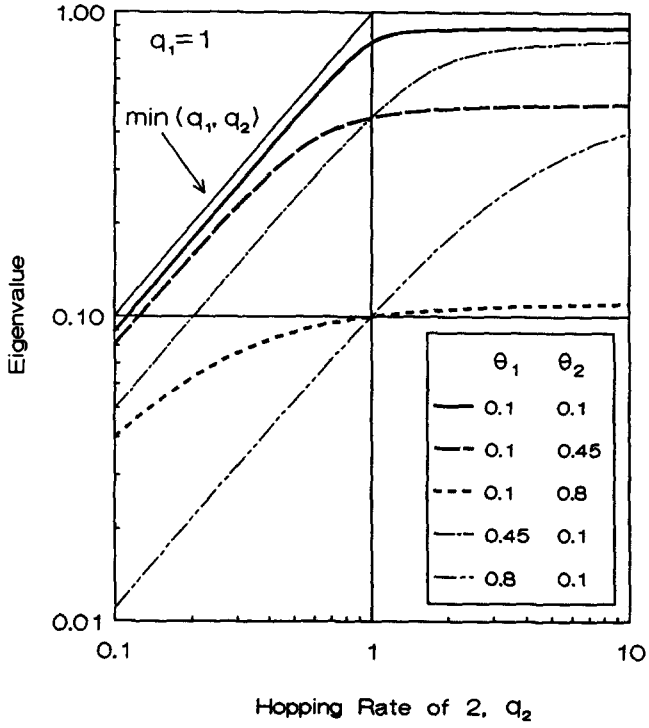

FIG. 9. The slow eigenvalue. Note that $0 \leq \lambda_s \leq \min(q_1, q_2)$.

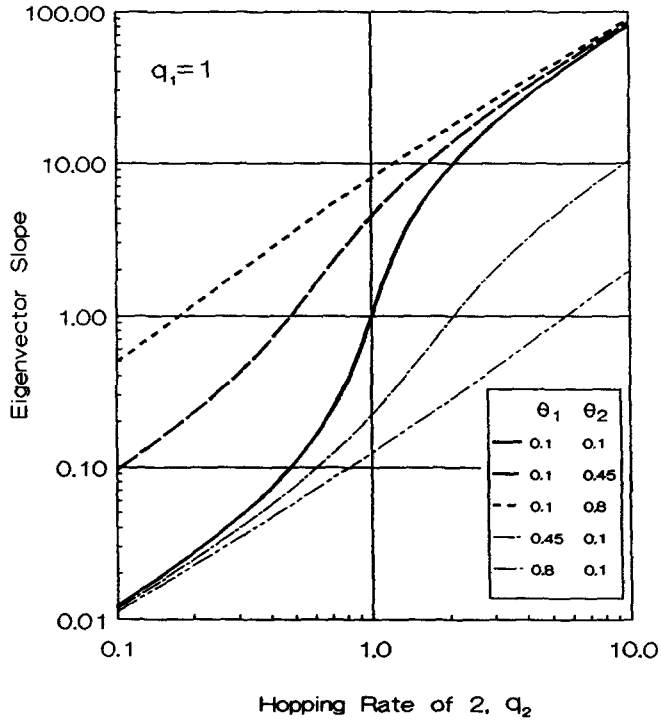

FIG. 10. The fast eigenvector slope.

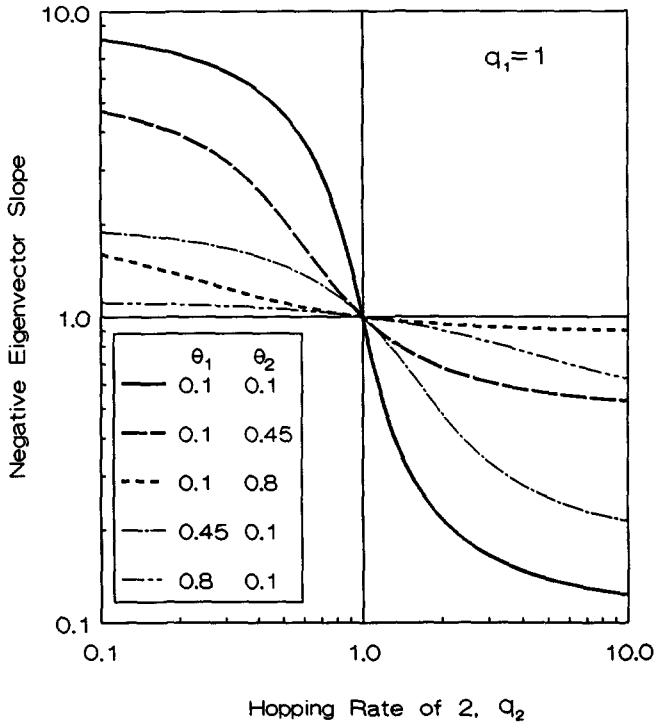

FIG. 11. The negative of the slow eigenvector slope.

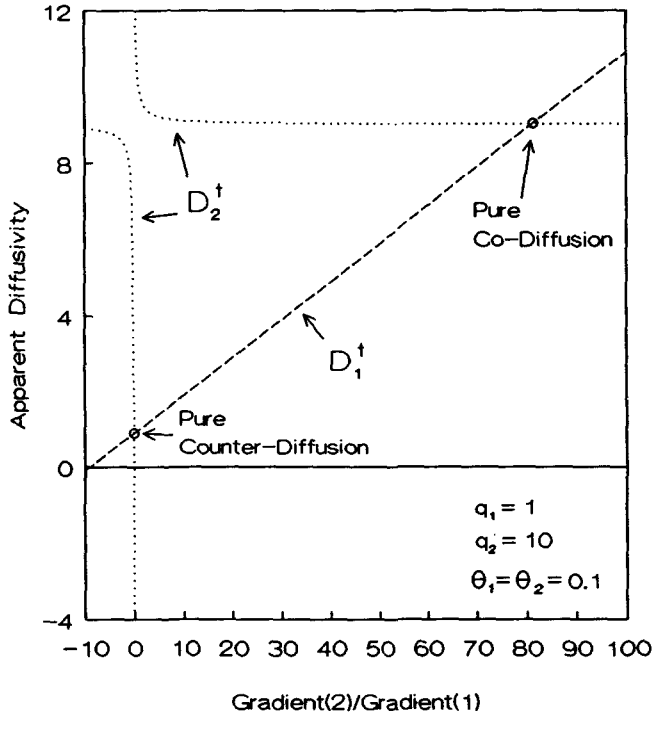

FIG. 12. Apparent diffusivities in the Wicke–Kallenbach cell for unequal hopping rates: $D_1^\dagger = 0.9 + 0.1[(d\theta_2/dx)/(d\theta_1/dx)]$; $D_2^\dagger = 9 + [(d\theta_1/dx)/(d\theta_2/dx)]$.

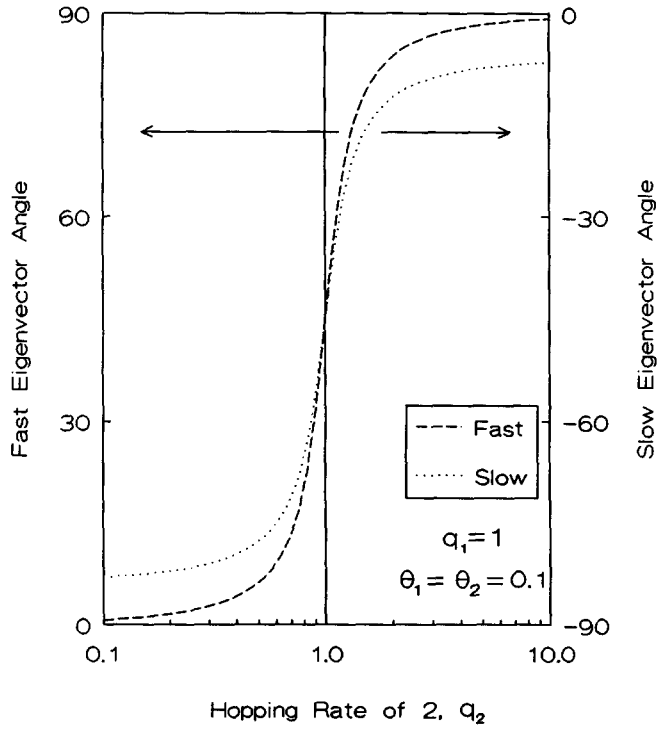

FIG. 13. The angles made by the slow and fast eigenvectors on the occupancy plane as a function of hopping rate.

co- and counterdiffusivities) increase with the hopping rate of component 2. For $q_2 \gg q_1$ the fast eigenvalue approaches an asymptote of $q_2(1 - \theta_1)$, as illustrated in Fig. 8, and the slow eigenvalue approaches $q_1(1 - \theta_1 - \theta_2)/(1 - \theta_1)$, as shown in Fig. 9. Similarly, for $q_2 \ll q_1$ the fast eigenvalue approaches $q_1(1 - \theta_2)$, and the slow eigenvalue approaches $q_2(1 - \theta_1 - \theta_2)/(1 - \theta_2)$. Therefore, when the two hopping rates differ greatly, pure codiffusion is driven by the hopping rate of the faster diffusing component and retarded by the occupancy of the slower component. Pure counterdiffusion is controlled by the hopping rate of the slower component and the occupancies of both components.

It can also be seen in Fig. 8 that the fast eigenvalue is bounded by $\min(q_1, q_2) \leq \lambda_f \leq \max(q_1, q_2)$, and in Fig. 9 that the slow eigenvalue is bounded by $0 \leq \lambda_s \leq \min(q_1, q_2)$. These results can be derived from Eqs. (27) and (28).

The change in hopping rates may also be interpreted as a rotation of eigenvectors, as alluded to in the section Illustrative Examples. Figure 13 shows the rotation of eigenvectors for the case $\theta_1 = \theta_2 = 0.1$ and $q_1 = 1$. The abscissa shows the value of q_2, and the ordinate shows the angle made by the eigenvectors with the $\nabla\underline{\theta} = (1, 0)$ axis on the θ_1, θ_2 plane. The tangent of this angle is equal to the eigenvector slope.

The relationship between the flux, the concentration gradients, and the eigenfunctions can be demonstrated in the following manner. We continue our eigenfunction representation of single-file diffusion in the Wicke–Kallenbach system by first expressing the concentration gradient vector in terms of the normalized fast and slow eigenvectors:

$$\nabla\underline{\theta} = C_f\underline{x}_f + C_s\underline{x}_s. \tag{30}$$

Now, to illustrate the effect of varying $\nabla\underline{\theta}$, let C_f and C_s vary, but with the restriction

$$C_f^2 + C_s^2 = 1. \tag{31}$$

This means that $\nabla\underline{\theta}$ circumscribes a circle on the $\underline{X}_f$, $\underline{X}_s$ plane, and so we take into account all possible gradient ratios. It follows from Eqs. (16) and (30) that

$$-\underline{J} = C_f\lambda_f\underline{x}_f + C_s\lambda_s\underline{x}_s, \tag{32}$$

and so

$$|\underline{J}| = C_f^2\lambda_f^2 + C_s^2\lambda_s^2 \tag{33}$$

which means, as illustrated in Fig. 14, that the locus of $-\underline{J}$ is an ellipse with a major axis of λ_f and a minor axis of λ_s. In this figure we are plotting $\underline{x}_f \cdot -\underline{J}$ and $\underline{x}_f \cdot \nabla\underline{\theta}$ on the abscissa, and $\underline{x}_s \cdot -\underline{J}$ and $\underline{x}_s \cdot \nabla\underline{\theta}$ on the ordinate. The $\nabla\underline{\theta}$ vector leads $-\underline{J}$ by an angle ω in the first and third quadrants, and lags by ω in the second and fourth quadrants. The angle ω is given by

$$\omega = \cos^{-1}\left[\frac{C_f^2\lambda_f + C_s^2\lambda_s}{C_f^2\lambda_f^2 + C_s^2\lambda_s^2}\right]. \tag{34}$$

The $\nabla\underline{\theta}$ and $-\underline{J}$ vectors coincide along the $\underline{X}_f$ and $\underline{X}_s$ directions, so that for $\nabla\underline{\theta} = \pm\underline{x}_f$, $-\underline{J} = \pm\lambda_f\underline{x}_f$, and for $\nabla\underline{\theta} = \pm\underline{x}_s$, $-\underline{J} = \pm\lambda_s\underline{x}_s$.

Transient Uptake: Constant Pressure

Another slightly more complicated example that can be considered is transient uptake in a constant pressure, infinite volume system. This situation arises, for example, in experiments done in an apparatus such as a Cahn balance. Only small perturbations of the gas phase are allowed. Now we have a transient system, instead of the steady-state system of the Wicke–Kallenbach scheme discussed earlier. This means that the diffusion equation must be considered in its entirety. We consider only the case where the hopping rates of the two components are equal to 1. Equations (20)–(22) can be solved analytically if we first diagonalize the diffusion matrix

$$\mathbf{D} = \mathbf{M}\mathbf{D}'\mathbf{M}^{-1} = \begin{bmatrix}\theta_1 & \theta_1\\ \theta_2 & -\theta_1\end{bmatrix}\begin{bmatrix}1 & 0\\ 0 & 1-\theta_1-\theta_2\end{bmatrix}\begin{bmatrix}1/(\theta_1+\theta_2) & 1/(\theta_1+\theta_2)\\ \theta_2/(\theta_1(\theta_1+\theta_2)) & -1/(\theta_1+\theta_2)\end{bmatrix} \tag{35}$$

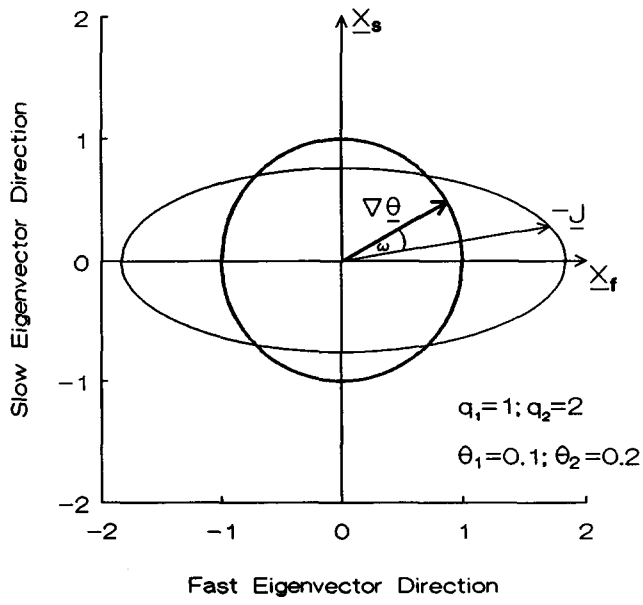

FIG. 14. The relationship between the flux and the concentration gradient vectors on the eigenvector plane.

and then transform the occupancy vectors

$$\theta' = \mathbf{M}^{-1}\underline{\theta} \tag{36}$$

to get a transformed equation

$$\frac{\partial\, \underline{\theta}'}{\partial t} = \mathbf{D}'\, \nabla^2\, \underline{\theta}' \tag{37}$$

with the boundary conditions also being transformed in the same manner. This system can be solved analytically, and transformed back to the original variables by

$$\underline{\theta} = \mathbf{M}\, \underline{\theta}'. \tag{38}$$

In a Cahn balance, or similar experiment, the diffusion coefficient is measured by perturbing the surface concentration and monitoring the approach to equilibrium. If it were possible to perturb the surface concentrations of the two components in equal and opposite directions then a state of pure counterdiffusion would exist, with the apparent diffusivities of both components being equal to the slow eigenvalue, $1 - \theta_1 - \theta_2$. Alternatively, if the concentrations of components 1 and 2 were perturbed in the ratio θ_1 to θ_2 then a state of pure codiffusion would exist, with the apparent diffusivities of both components being equal to the fast eigenvalue, 1. Thus, in these special cases, Fig. 3 once again applies and gives the occupancy dependency of pure codiffusion and pure counterdiffusion.

Experimentally, however, it is difficult to achieve the perturbations that give the simplest mathematical result. In particular, it may not be possible to set up a pure counterdiffusion system. A perturbation caused by simply increasing the surface concentration of one component, though, may be more easily possible. In this case there will be a decrease in the surface concentration of the other component through the interplay of the Langmuir equilibrium isotherm. If an infinitesimal amount of component 1 is injected into the system, it can be shown that

$$-1 < \frac{d\theta_2}{d\theta_1} = \frac{\theta_2}{\theta_1 - 1} < 0, \tag{39}$$

where

$$\theta_1 + \theta_2 \leq 1.$$

This means that the decrease in the occupancy of component 2 will always be less than the increase in occupancy of component 1. It follows that, in general, the concentration gradient of component 2 is going to be in the opposite direction and smaller than the concentration gradient of component 1.

Consider the case where there is no initial component 1 present. We use the methodology described above to calculate the apparent diffusion coefficient for each component when an infinitesimal amount of component 1 is injected into the system which initially contains only component 2. Figure 15 shows the apparent diffusivities of each component as a function of the initial amount of component 2 present. It can be seen that $D_1^\dagger$ decreases as $(1 - \theta_2)$. Also, $D_2^\dagger$ is smaller than $D_1^\dagger$ due to the component 2 gradient being smaller and in the opposite direction to the gradient of component 1. This last observation can be related to the result described previously in Fig. 7, where it can be seen that when $-1 <$ gradient(2)/gradient(1) < 0, then the apparent diffusivity of component 2 is smaller than that of component 1.

Figure 16 shows an example of the fitting of the apparent diffusivities of Fig. 15. It can be seen that for component 1 the fitted curve matches the model's uptake curve exactly. This occurs because the component going in is generated by only one eigenvalue. For component 2, which is coming out, the fitted curve does not match the theoretical curve exactly, since it is generated from a mixture of the two eigenvalues.

Transient Uptake: Variable Pressure (Constant Volume)

Qureshi and Wei (*19*) collected two-component diffusion data in a constant volume, variable pressure apparatus. In those experiments, a mass balance of chemical species between the gas and adsorbed phases

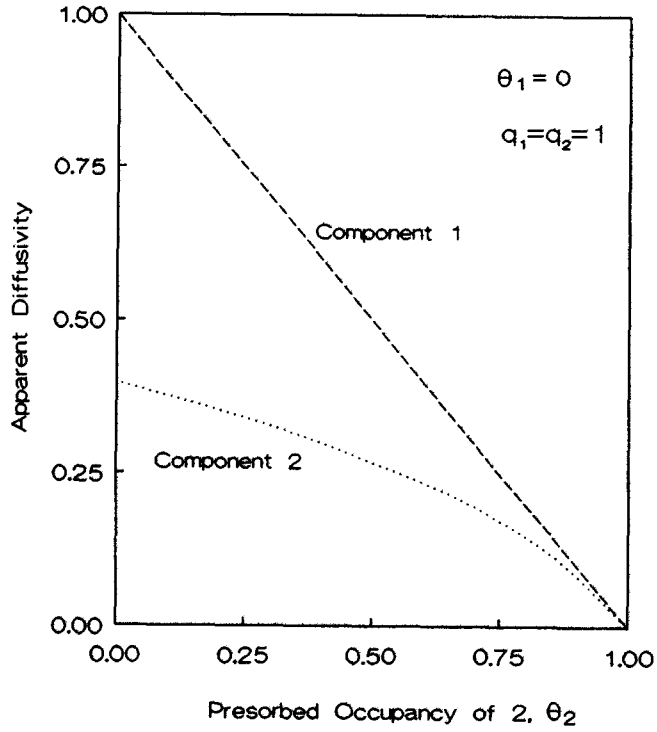

FIG. 15. Apparent diffusivities for a Transient Uptake, Constant Pressure experiment with an infinitesimal amount of component 1 injected (counterdiffusion conditions).

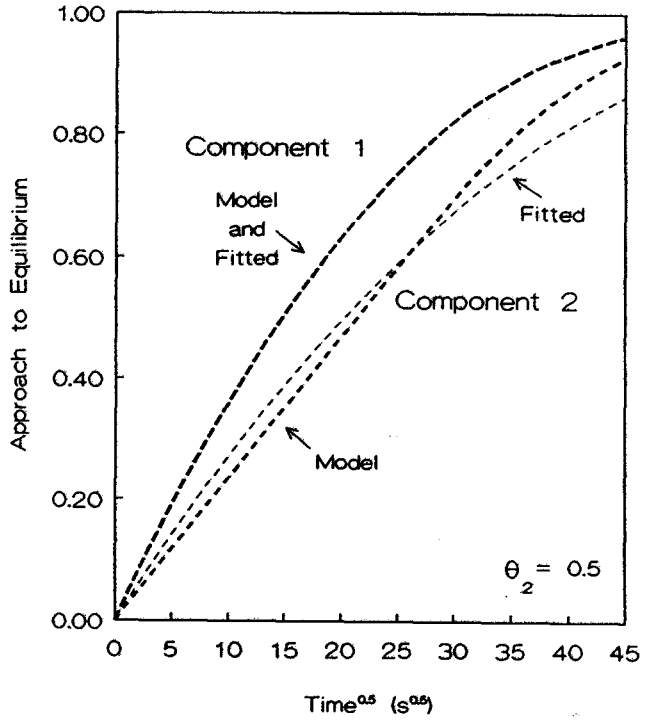

FIG. 16. Sample calculation of apparent diffusivities for Fig. 15.

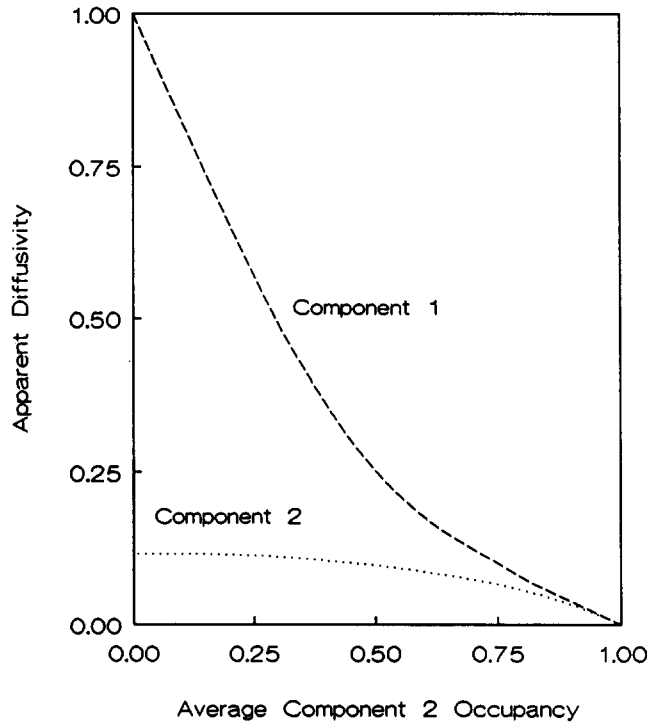

FIG. 17. Apparent diffusivities for a Transient Uptake, Variable Pressure (Constant Volume) experiment with a finite amount of component 1 injected (counterdiffusion conditions).

played a role. In addition, for experimental reasons, nonnegligible amounts were injected into the system. This system was analyzed using Langmuir isotherm boundary conditions and a mass balance between the adsorbed and gas phases as described in the section on apparent diffusivity. The system had to be analyzed numerically.

An example of the results is shown in Fig. 17, with the input parameters given in Table 1. The general trends of the constant pressure results of Fig. 15 are still followed in this more realistic case. Component 1, which is being adsorbed, shows an almost linear decrease in apparent diffusion coefficient with an increasing amount of component 2 presorbed in the catalyst. Component 2, which is being desorbed, shows a very low apparent diffusion coefficient, and, in general, it is much lower than the apparent diffusion coefficient of component 1. Both sets of apparent diffusion coefficients approach zero at high occupancy. The apparent diffusivities are functions of several parameters, including the amount of component 2 present, the amount of

TABLE 1

Parameters Used in Transient Uptake, Variable Pressure Simulation of Fig. 17

q_1	1.0
q_2	0.6875
K_1	0.113 Pa^{-1}
K_2	0.0270 Pa^{-1}
V_g	205 cm^3
m	0.005 g
ρ	5.77×10^{-4} mol g^{-1}
P_{1in}	32 Pa
P_{2in}	0 Pa
T	338 K

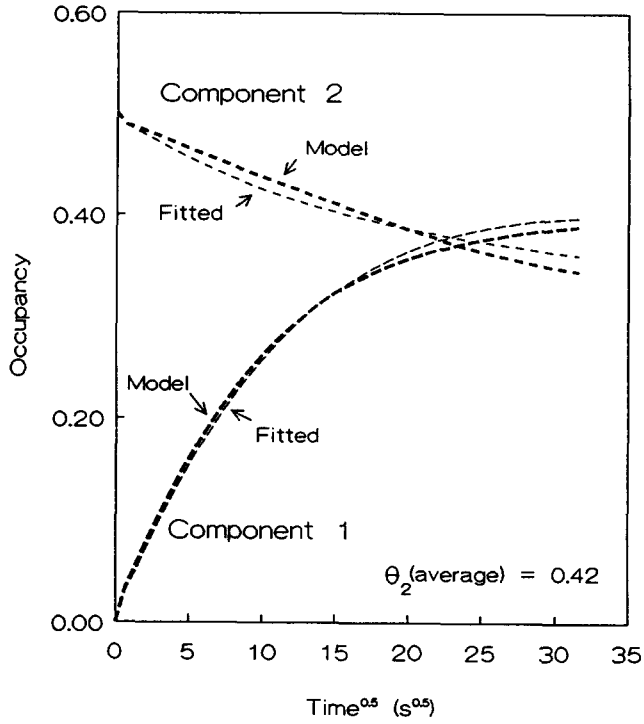

FIG. 18. Sample calculation of apparent diffusivities for Fig. 17.

component 1 injected, and the Langmuir isotherm constants. The apparent diffusivity of component 2 is so low at least partly because a finite amount of component 1 is being injected, whereas, in Fig. 15 an infinitesimal amount was injected. Figure 18 shows an example of the calculation of apparent diffusivities for Fig. 17.

First-Order, Reversible Reaction

Finally, consider the case of a first-order reversible reaction at steady state. It is possible to analyze this system analytically if it is assumed that the hopping rates of the two components are equal. Then for slab geometry, with x going from 0 at the center to L at the surface,

$$\frac{d}{dx}\left[\mathbf{D}\frac{d}{dx}\underline{\theta}\right] = \mathbf{K}\underline{\theta}, \tag{40}$$

where

$$\mathbf{D} = \alpha^2 q \begin{bmatrix} (1-\theta_2) & \theta_1 \\ \theta_2 & (1-\theta_1) \end{bmatrix} \tag{41}$$

and

$$\mathbf{K} = \begin{bmatrix} k_1 & -k_2 \\ -k_1 & k_2 \end{bmatrix}. \tag{42}$$

Here, q is the hopping rate of each component, and k_1 and k_2 are the forward and reverse reaction rates. The boundary conditions specify the surface concentrations of each component, as well as the symmetry condition at the centerline:

$$\theta_i = \theta_{ib} \quad \text{at } x = L;\ i = 1, 2 \tag{43}$$

$$\frac{d\theta_i}{dx} = 0 \quad \text{at } x = 0;\ i = 1, 2. \tag{44}$$

The solution of this system of equations is

$$\theta_i = \left[\theta_{ib} - \frac{k_j\theta}{k_1 + k_2}\right] \times \frac{\cosh\left[\sqrt{\dfrac{k_1 + k_2}{\alpha^2 q(1-\theta)}}\, x\right]}{\cosh\left[\sqrt{\dfrac{k_1 + k_2}{\alpha^2 q(1-\theta)}}\, L\right]} + \frac{k_j\theta}{k_1 + k_2}, \tag{45}$$

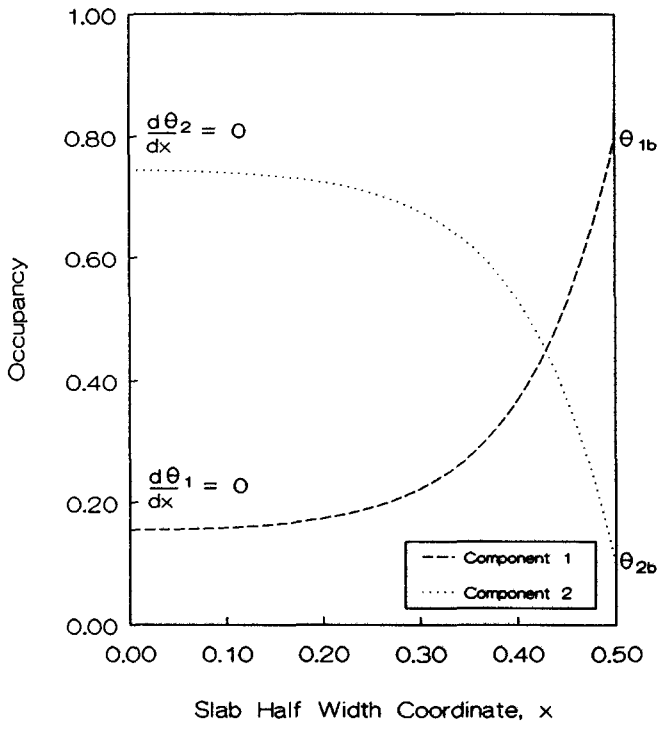

FIG. 19. Example of occupancy profiles for a First-Order Reversible Reaction.

where $i = 1, 2; j = 1, 2; j \neq i$; and $\theta = \theta_1 + \theta_2$ is not a function of x.

The effectiveness factor is given by

$$\eta = \frac{1}{L(k_1\theta_{1b} - k_2\theta_{2b})} \int k_1\theta_1 - k_2\theta_2 \, dx$$

$$= \frac{\tanh \phi}{\phi}, \tag{46}$$

where

$$\phi = \sqrt{\frac{k_1 + k_2}{\alpha^2 q(1 - \theta)}}\, L. \tag{47}$$

It follows that the effectiveness factor valid for any geometry, for the diffusion limited case is given by

$$\eta_\infty = 1/\Phi, \tag{48}$$

where the modulus Φ is defined by

$$\Phi = \frac{V_p}{S_p} \sqrt{\frac{k_1 + k_2}{\alpha^2 q(1 - \theta)}}. \tag{49}$$

Here, V_p/S_p is the volume to surface area of the particular geometry being considered.

Comparison of Eqs. (47) and (49) with the usual expressions for the Thiele modulus shows that the single-file counterdiffusion model predicts that this two-component system will diffuse with an effective diffusivity given by

$$D_e = \alpha^2 q(1 - \theta). \tag{50}$$

This means that in the diffusion limited regime, the effect of occupancy is to reduce the effectiveness factor by a factor of $\sqrt{(1 - \theta)}$.

Figure 19 shows an example of such a reaction, where $\theta_{1b} = 0.8$, $\theta_{2b} = 0.1$, $\alpha^2 q_1 = 1$, $\alpha^2 q_2 = 1$, $k_1 = 10$, $k_2 = 2$, and $L = 0.5$.

As Eq. (50) shows, the diffusivity for each component calculated for this reacting system turns out to be the same as the self-diffusivity of a single component with hopping rate q and occupancy θ in a nonreacting system. This result occurs because, in the reaction system considered, the fluxes and gradients of the two components are

always equal in magnitude and opposite in sign.

CONCLUSIONS

The diffusion matrix has a fast eigenvalue, $\lambda_f \geq 0$, a slow eigenvalue, $\lambda_s \geq 0$, and the properties:

- The fast eigenvalue is bounded by $\min(q_1, q_2) \leq \lambda_f \leq \max(q_1, q_2)$.
- The slow eigenvalue is bounded by $0 \leq \lambda_s \leq \min(q_1, q_2)$.
- For one hopping rate much bigger than the other, the fast eigenvalue is driven by the hopping rate of the faster component and retarded by the occupancy of the slower component. The slow eigenvalue is controlled by the hopping rate of the slower component and both occupancies.

In the Wicke–Kallenbach case:

- The fast mode is interpreted as a case of codiffusion (fluxes in the same direction), and the slow mode as a case of counterdiffusion (fluxes in opposite directions). We call these two states pure codiffusion and pure counterdiffusion since they correspond to pure modes of the diffusion matrix.
- The apparent diffusivities of both components are always less than their respective intrinsic hopping rates when the concentration gradients of the two components are in opposite directions.

For transient uptake:

- The apparent diffusivity for transient uptake problems was defined so as to create a practical method of comparing theory with experimental results.
- The apparent diffusivity of the component going in is greater than that for the component coming out since the concentration gradient of the injected component is larger.

For a first-order reversible reaction:

- In the diffusion limited regime, and for equal hopping rates, the effect of occupancy is to reduce the effectiveness factor by a factor of $\sqrt{(1 - \theta)}$.

APPENDIX: NOMENCLATURE

Variables

C_f	Scalar defined by Eq. (12)
C_s	Scalar defined by Eq. (12)
$\mathbf{D}$	Constitutive diffusion matrix
$\mathbf{D}'$	Transformed diffusion matrix
$\mathbf{D}^\dagger$	Apparent diffusivity matrix
D	One-component diffusivity ($cm^2\ s^{-1}$)
$D_i^\dagger$	Apparent diffusivity of component i ($cm^2\ s^{-1}$)
$\underline{J}$	Flux vector
J_i	Flux of ith component
$\mathbf{K}$	Reaction rate matrix
K_i	Langmuir isotherm constant (Pa^{-1})
k_i	Reaction rate constant (s^{-1})
L	Slab half-width (cm)
$\mathbf{M}$	Diagonalizing matrix
m	Mass of crystals (g)
P_i	Partial pressure of ith component (Pa)
$P_{i\,in}$	Increase upon injection of partial pressure of ith component (Pa)
p	Bombardment rate of a molecule onto the grid boundary (s^{-1})
p_i	Bombardment rate of ith component onto the grid boundary (s^{-1})
q	Hopping rate of a molecule to a specific adjacent site, in an otherwise empty lattice (s^{-1})
q_i	Hopping rate of a molecule of the ith component to a specific adjacent site, in an otherwise empty lattice (s^{-1})
R	Crystal radius (cm)
R_g	Gas-law constant ($Pa\ cm^3\ mol^{-1}\ K^{-1}$)
r	Radial coordinate (cm)
T	Temperature (K)
t	Time coordinate (s)
V	Volume of crystals (cm^3)
V_g	Gas phase volume (cm^3)
$\underline{X}$	Eigenvector
$\underline{x}$	Normalized eigenvector
x	Slab half-width coordinate (cm)

Greek

- α Distance between grid intersections (cm)
- η Effectiveness factor for slab geometry
- η_∞ Effectiveness factor for any geometry, diffusion limited case
- $\underline{\theta}$ Occupancy vector
- $\underline{\theta}'$ Transformed occupancy vector
- $\nabla\underline{\theta}$ Occupancy gradient vector
- $\bar{\theta}$ Volumetric average occupancy (molecules/intersection)
- θ_i Occupancy of component i (molecules/intersection)
- θ Total occupancy or occupancy in one-component system (molecules/intersection)
- $\nabla\theta_i$ Gradient of component i
- λ Eigenvalue
- ρ Moles of intersections per gram of catalyst (mol g^{-1})
- Φ Thiele Modulus for any geometry
- ϕ Thiele Modulus for slab geometry
- $\chi_i(t)$ Approach to equilibrium curve for ith component
- ω Angle between $\nabla\underline{\theta}$ and $-\underline{J}$ vectors

Subscripts

- f Fast eigenvalue
- i ith component
- ib Boundary condition of ith component
- i_0 Initial condition for ith component
- $i\infty$ Equilibrium condition for ith component
- s Slow eigenvalue

Superscripts

- $'$ Transformed diffusion matrix or occupancy vector
- † Apparent diffusivity or apparent diffusivity matrix

REFERENCES

1. Barrer, R. M., and Jost, W., *Trans. Faraday. Soc.* **45,** 928 (1949).
2. Habgood, H. W., *Canad. J. Chem.* **36,** 1384 (1958).
3. Riekert, L., *AIChE J.* **17,** 446 (1971).
4. Palekar, M. G. and Rajadhyaksha, R. A., *Chem. Eng. Sci.* **40,** 1085 (1985).
5. Palekar, M. G., and Rajadhyaksha, R. A., *Chem. Eng. Sci.* **40,** 663 (1985).
6. Palekar, M. G., and Rajadhyaksha, R. A., *Chem. Eng. Sci.* **41,** 463 (1986).
7. Theodorou, D., and Wei, J., *J. Catal.* **83,** 205 (1983).
8. Tsikoyiannis, J. G., Ph.D. thesis, Massachusetts Institute of Technology, 1986.
9. Tsikoyiannis, J. G., and Wei, J., *Chem. Eng. Sci.* (1990).
10. Sundaresan, S., and Hall, C. K., *Chem. Eng. Sci.* **41,** 1631 (1986).
11. Nagy, J. B., Derouane, E. G., Resing, H. A., and Miller, G. R., *J. Phys. Chem.* **87,** 833 (1983).
12. Eckman, R. R., and Vega, A. J., *J. Phys. Chem.* **90,** 4679 (1986).
13. Kustanovich, I., Fraenkel, D., Luz, Z., Vega, S., and Zimmermann, H., *J. Phys. Chem.* **92,** 4134 (1988).
14. Mentzen, B. F., *Mater. Res. Bull.* **22,** 337 (1987).
15. Mentzen, B. F., and Bosselet, F., *Mater. Res. Bull.* **23,** 227 (1988).
16. Derouane, E. G., *J. Catal.* **100,** 541 (1986).
17. Derouane, E. G., Nagy, J. B., Fernandez, C., Gabelica, Z., Laurent, E., Maljean, P., *Appl. Catal.* **40,** L1 (1988).
18. Moore, R. M., and Katzer, J. R., *AIChE J.* **18,** 816 (1972).
19. Qureshi, W. R., and Wei, J., *J. Catal.* **126,** 147 (1990).